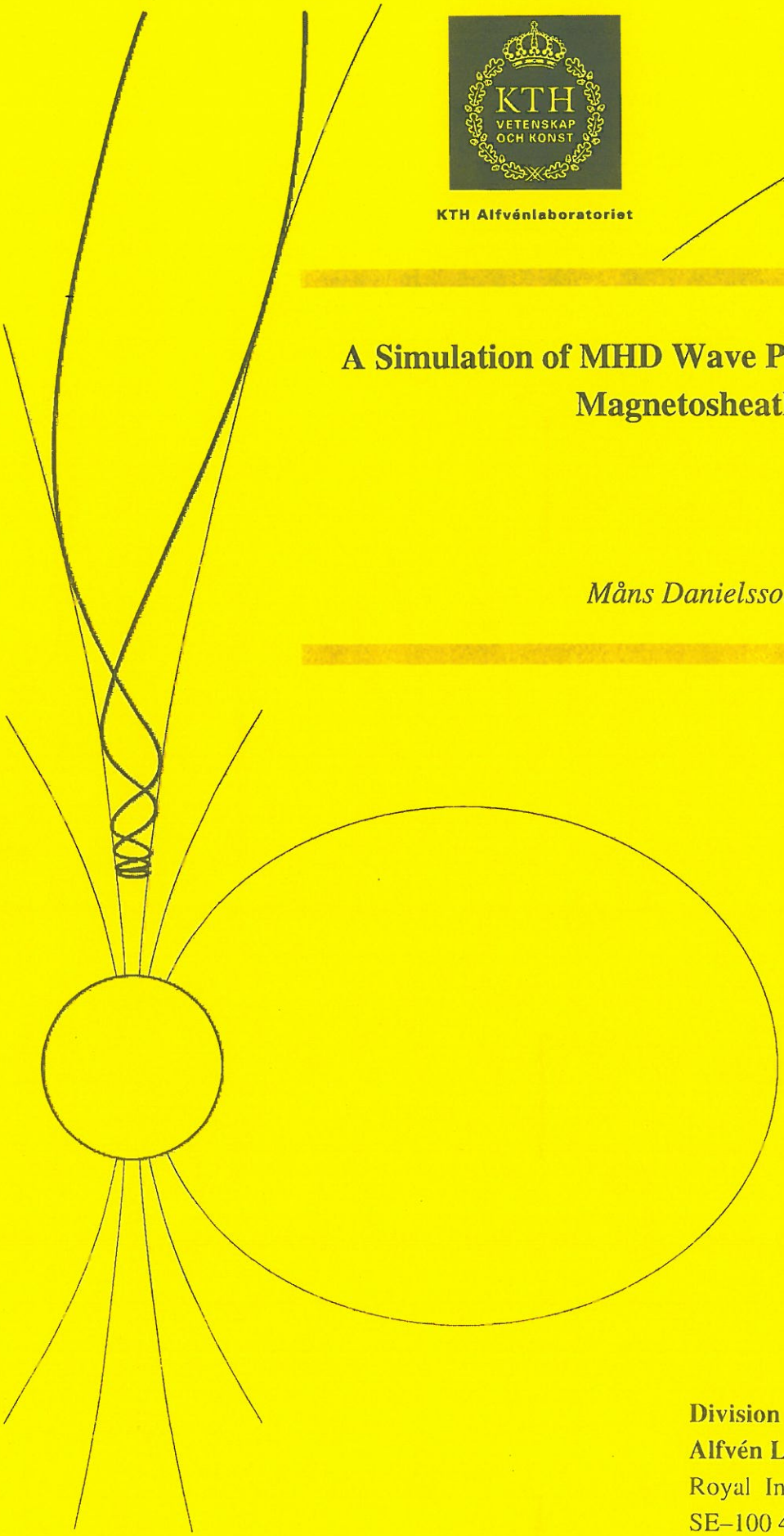

KTH Alfvénlaboratoriet

ALP-2003-104

A Simulation of MHD Wave Propagation in the Magnetosheath

Måns Danielsson

Division of Plasma Physics
Alfvén Laboratory
Royal Institute of Technology
SE–100 44 Stockholm, Sweden

A Simulation of MHD Wave Propagation in the Magnetosheath

Måns Danielsson

Abstract

A set of ray tracing equations for MHD wave propagation in a moving media is described, together with the basics of wave physics and ray tracing. A method for how these equations can be used to model the propagation of a disturbance in the solar wind from the bow shock to the magnetopause is developed. This method is implemented, using simple linear models for the background fields and a hydrodynamic flow model for the plasma flow. The program is then run for a few configurations and the result is presented.

KTH Report ALP-2003-104

Contents

1 Introduction

1.1 The Magnetosphere and the Solar Wind

The magnetic field surrounding Earth, with poles approximately coinciding with the geographic poles, derives from electric currents inside Earth. Close to Earth, where the field is strong and undisturbed by other magnetic sources, it resembles the field from a magnetic dipole. Further out, however, it changes under the influence of the solar wind, a flow of ionized particles coming from the Sun. This electrically conducting gas, or plasma, permeats the whole solar system, deforms the geomagnetic field into a small cavity in the interplanetary field, and is the cause of a multitude of electromagnetic phenomena in Earth's vicinity, e.g., auroras and magnetic storms.

The cavity in the solar wind in which the geomagnetic field is dominating, is called the magnetosphere. This area of space, which was first believed to be very simple, is now known to consist of a complex structure of plasma populations, interacting with the magnetic field. This interaction is not only electromagnetic, but is also governed by the laws of gas dynamics. The solar wind hits the geomagnetic field at supersonic speed and a shock front is created, resembling the shock front in the atmosphere ahead of a jet plane. This so called bow shock represents the transition from supersonical to subsonical flow in the solar wind. Inside the bow shock there is a region of subsonically flowing plasma, the magnetosheath, where the plasma flows around the magnetosphere.

The boundary between the magnetosheath and the region where the geomagnetic field is dominating is called the magnetopause. This is the outer boundary of the magnetosphere. The inner boundary is the ionosphere. In this layer, about $100-300$ km above ground, ultraviolet and soft X-ray radiation from the sun ionizes molecules from the atmosphere. This means that the ionosphere is electrically conducting, and may reflect electromagnetic waves.

Figure 1 shows the structure of the magnetosphere. The regions we deal with here are mainly the bow shock, the magnetosheath and the magnetopause, to see how waves in the solar wind, refracted by the bow shock, are propagated inside the magnetosheath.

1.2 Magneto-Hydrodynamic Waves

A plasma is a gas containing a significant number of electrically charged particles. Because it is a gas, its motion is governed by the laws of gas dynamics. But it is also electrically charged, and is therefore affected by the laws of electrodynamics. The motion of the plasma affects the charge distributions and the currents and distorts the magnetic field lines. When the electrons and ions of a plasma are displaced relative their equilibrium position, a charge imbalance is induced, and the particles are affected by a

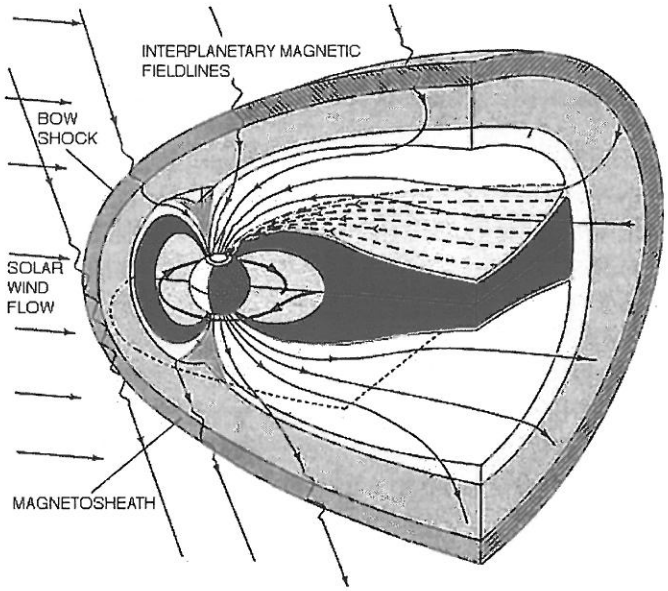

Figure 1: The structure of the magnetosphere.

restoring force by the electromagnetic field. A number of natural frequencies are therefore associated with a plasma consisting of certain electron and ion populations, and these frequencies play an important role in the wave equations of plasma motion.

When a magnetic field is present in a plasma, this interaction between the laws of gas dynamics and Maxwell's equations give rise to a kind of waves unique to plasma motion, where spatial perturbations of the particles and oscillations in the electromagnetic fields couple in a very intricate way. These waves are called magneto-hydrodynamic (MHD) waves, or Alfvén waves after their discoverer Hannes Alfvén. The conditions that characterize MHD wave propagation, and that are expressed in the governing equations, allow for a number of different ways for perturbations, mechanical and electromagnetic, to propagate. We distinguish between *compressional* waves, where disturbances in mass density and magnetic flux density are propagated, and *shear Alfvén* waves, which carry a perturbation magnetic field, without changing the plasma density or pressure. Furthermore, there are different types of compressional and shear Alfvén waves. We shall be concerned mainly by the type of compressional wave called the fast wave, since this is the only mode that can carry a significant amount of energy perpendicularly to the magnetic field ([6]), which is the direction we shall limit ourselves to in this investigation, for reasons of simplicity of the equations.

A shear Alfvén wave, propagating parallel to a magnetic background magnetic field $\mathbf{B}$, does so with a certain phase velocity, called the *Alfvén*

velocity $\mathbf{V}_A$:

$$\mathbf{V}_A = \frac{\mathbf{B}}{\sqrt{\mu_0 \rho_m}} \tag{1}$$

where ρ_m is the mass density of the plasma medium and μ_0 is the magnetic permeability of free space. This velocity plays an important role in all wave equations and dispersion relations for plasma waves, as we see later in this report.

1.3 Field Line Resonances in the Magnetosphere

Ultra-low frequency (ULF) fluctuations in the geomagnetic field have been observed on the ground since the first measurements in the nineteenth century. Some are continuous, quasi-sinusoidal pulsations, and these are grouped into the so called Pc pulsations, from Pc-1 ($0.2 - 5$ Hz) to Pc-5 ($1.7 - 6.7$ mHz). The periods and the distinct frequency peaks of these pulsations suggest that they are deriving from resonances in the geomagnetic field, i.e., standing MHD waves along the field lines that are reflected at the ionosphere, and partly transmitted down to the surface of the Earth. This theory has been developed since the fifties, and is further supported by both ground based and satellite borne observations ([13]).

For these resonances to occur, the waves must satisfy certain boundary conditions. The boundaries consist of the ionosphere, which in this case can be viewed as a thin conducting sheet, and the magnetopause. To be perfectly reflected at the ionosphere at the ends of the field line, the wave along that field line must have a vanishing electric field and displacement there. The strongest resonance will therefore occur for wavelengths which satisfy

$$\lambda_{||} = \frac{2l}{n} \tag{2}$$

where $\lambda_{||}$ is the wavelength along the field direction, l is the length of the field line and n is an integer. This suggests that a perturbation in a magnetic field line inside the magnetosphere, initialized at the magnetopause, could create Alfvén waves with certain frequencies, standing along this field line. The frequencies are determined by the length of the field line, the strength of the geomagnetic field, and the plasma density. In the same way, a pressure perturbation could excite compressional waves. These waves (the Alfvén and the fast) would then result in the measured Pc pulsations at ground level ([6]).

1.4 The Source of Field Line Resonances

The structure of Pc-5 field line resonances in the geomagnetic field is well explained and documented. The source, however, is still subject of discussion. As a wave, propagating through the magnetopause, comes closer to

Earth, the Alfvén speed increases, and a turning point, where the wave is reflected, is eventually reached. One theory states that a region between the magnetopause and this turning point acts as a resonant cavity, in which incident waves in the solar wind could excite oscillations with the natural frequencies of this cavity. These oscillations would then in turn excite the field line resonances at discrete frequency intervals. It has been observed, however, that the resonances occur at very stable frequencies: $1.3, 1.9, 2.6$ and 3.3 mHz. This means that the dimensions of the cavity must be more or less stable which is not plausible, noting the extremely dynamic nature of the magnetosphere. For example, the distance between the Earth and the magnetopause on the sunward side may vary by several Earth radii under the pressure of the solar wind.

Instead, a model were the Pc-5 resonances are directly driven by MHD waves in the solar wind has been proposed ([5]). The waves, passing through the bow shock, propagate through the magnetosheath until they reach a magnetospheric field line with matching natural frequencies. At that point they excite a resonance along the field line. Observations of oscillations in the solar wind and Pc-5 pulsations in the magnetosphere have been made which agree with this theory, and further studies are in progress.

1.5 The Object

In the effort to clarify the mechanisms behind the geomagnetical pulsations, and to achieve a more complete description of the dynamics of the magnetosphere, it is of interest to analyze how disturbances in the solar wind are transmitted through the bow shock, how they propagate in the magnetosheath, and if and how they reach the magnetopause to be transmitted or reflected. This has previously been done analytically, using a box model of the magnetosphere ([1], [2]), but since the equations governing MHD wave propagation in the plasma surrounding Earth are quite complex, numerical methods has to be employed for more realistic geometries. An extensive work was carried out in the 1970's by John Spreiter and others ([14], [7]). This advanced project is however hard to apply to the problem in focus in this paper.

A set of previously developed ray tracing equations, together with some crude approximations and models of the background quantities, are implemented. The most important approximations are:

1. Geometry: the bow shock is approximated as a parabola and the magnetosphere as a sphere. This should be no great impediment, since the geometry of the magnetosphere is very dynamic anyway.

2. Plasma flow: we assume incompressible gas-dynamic flow around a sphere, and ignore the magnetic pressure. This leads to inconsisten-

cies in the model if a magnetic field is introduced, and restricts us to investigating the nose of the bow shock, where the flow is subsonic.

3. Magnetic field: The magnetic field is held constant, or even set to zero to retain consistency of the model. The presence of a magnetic field in the magnetosheath makes the gas-dynamic flow model invalid.

By implementing these equations, paying attention to generality and easy extendability, and evaluating the validity and consistency of the implementation, I hope to take a small step towards creating a more advanced program for simulation of MHD wave propagation in the magnetosheath.

1.6 A Word on Notation

As it is more effective programming to use matrix and vector computations whenever possible, instead of doing calculations component wise, I shall stick to using matrix notation instead of the sometimes more convenient suffix notation. The following conventions are used throughout the report:

1. All vectors are column vectors if not otherwise stated: $\mathbf{r} = (r_1, r_2, \ldots, r_n)^T$.
2. $\frac{\partial \alpha}{\partial \mathbf{r}}$ indicates the vector $(\frac{\partial \alpha}{\partial r_1}, \frac{\partial \alpha}{\partial r_2}, \cdots, \frac{\partial \alpha}{\partial r_n})^T$.
3. $\frac{\partial \mathbf{r}}{\partial t}$ indicates the vector $(\frac{\partial r_1}{\partial t}, \frac{\partial r_2}{\partial t}, \cdots, \frac{\partial r_n}{\partial t})^T$.
4. $\frac{\partial \mathbf{k}}{\partial \mathbf{r}}$ indicates the matrix $\mathbf{D}$ where $D_{ij} = \frac{\partial k_i}{\partial r_j}$, the Jacobian of $\mathbf{k}$.
5. $\frac{\partial^2 \alpha}{\partial \mathbf{r}^2}$ indicates the symmetric matrix $\mathbf{D}$ where $D_{ij} = \frac{\partial^2 \alpha}{\partial r_i \partial r_j}$.

2 The Mathematical Background

In Chapter 1 a simple and intuitive description of plasma and plasma behaviour was given. Here, we go into more detail and describe the mathematical basics of plasma physics and ray tracing. But let us first mention some basic concepts of wave physics.

2.1 Waves and Wave Velocity

A localized disturbance of the equilibrium state of a physical quantity, such as a gas or a magnetic field, transported through it with a finite speed, is what we call a wave. This phenomenon can be mathematically described by an integral of exponential functions:

$$A(\mathbf{r}, t) = \int_{-\infty}^{\infty} \Psi(\mathbf{k}) \exp[i\phi(\mathbf{k})] d^3\mathbf{k} \tag{3}$$

Each infinitesmal element in the integral represents a separate wave, oscillating harmonically with its own wavelength and frequency, interfering with the others to form the resulting wave. All this is basic Fourier analysis, see [9].

The velocity with which a surface of constant phase propagates is called the phase velocity of the wave. In the case of the simple wave represented by a single exponential function the phase velocity, given by the equation

$$\frac{\partial \phi}{\partial t}(\mathbf{r}, \mathbf{k}, t) = 0, \tag{4}$$

is easy to understand and make sense of. But what do we mean when we talk about the phase and phase velocity of the total wave, consisting of the sum of possibly infinitely many sinusoidal waves, each moving with its own phase velocity?

In the integral (3), we assume that the amplitude function Ψ has a sharp peak at $k = k_0$, which is the case for a wave with a well defined frequency. This means that the integrand is everywhere zero except in a neighbourhood of k_0, around which it oscillates antisymmetrically. At a point in space where the phase depends strongly on $\mathbf{k}$, there will be cancellation and no significant contribution will be made to the integral. The component waves are not in phase and interfere destructively. Only where the phase does not depend on the components of $\mathbf{k}$, so that

$$\frac{\partial \phi}{\partial \mathbf{k}}(\mathbf{r}, \mathbf{k}, t) = 0, \tag{5}$$

will constructive interference and a strong contribution to the integral (3) occur. The point where this condition is satisfied represents in some sense the mean value of the wave disturbance. It moves through space with a velocity which we call the group velocity of the wave, as it is composed of the velocities of a group of simpler waves. This velocity is aligned with and closely linked to the velocity with which energy is transported by the wave, see [3] for details. In the next chapter, we will derive numerically integrable equations for the propagation of this point, and use them to trace its path through the magnetosheath for some different configurations.

For a detailed investigation of wave energy, see [4]

2.2 Fundamental Plasma Equations

The fundamental equations governing the behaviour of the plasma particles are ([3]):

1. Maxwell's equations, describing the currents and charge distributions in the plasma.

2. Constitutive relations, relating the variables in Maxwell's equations to each other. For example, the conductivity of the media relates the electric field to the current density.

3. Lorentz Force Law, which gives the force imposed on a single particle by the electromagnetic field.

To obtain an equation of motion for the plasma from these relations we cannot describe the motion of every single particle. Instead, we consider some average motion of a collection of particles. How this averaging procedure is performed is a matter of what approximations are appropriate for the problem, see [13].

If the thermal motion of the plasma is negligible compared to the motion imposed by the wave perturbation, one can assume that an unperturbed particle is at rest. We can treat a fluid volume element δV as a continuum, governed by Lorentz Force Law: $m\dot{\mathbf{v}} = q(\mathbf{E} + \mathbf{v} \times \mathbf{B})$. This is called the cold plasma approximation. When the thermal motion is small, but not negligible, we may use the same approximation by including the effects of temperature and pressure. The basis for this work will be a set of linearized equations taken from [3]: the momentum equation, with thermal motion included as of above,

$$\rho_m\{\frac{\partial}{\partial t} + \mathbf{V} \cdot \nabla\}\mathbf{v} = \mathbf{j} \times \mathbf{B} - \nabla p; \tag{6}$$

a combination of the continuity equation and the adiabatic law,

$$\frac{dp}{dt} = -\rho_0 V_S^2 \nabla \cdot \mathbf{v}; \tag{7}$$

Faradays law,

$$\nabla \times \mathbf{E} = -\frac{\partial \mathbf{b}}{\partial t}; \tag{8}$$

Ampèrés law,

$$\nabla \times \mathbf{b} = -\mu_0 \mathbf{j}; \tag{9}$$

and Ohm's law with infinite conductivity,

$$\mathbf{E} + \mathbf{v} \times \mathbf{B} + \mathbf{V} \times \mathbf{b} = 0, \tag{10}$$

where $\mathbf{v}, \mathbf{b}, \mathbf{E}, \mathbf{j}$ and p are the first-order wave perturbations of the background fields $\mathbf{V}, \mathbf{B}, \mathbf{E_0}, \mathbf{J}$ and P. From these equations a dispersion relation can be derived, which in turn will form the basis of our ray tracing equations.

In this work, collisions between particles are not considered. In a plasma where a significant number of particles are neutral, the equations of motion

must include the effects of collisions between the ions and the neutrals. Likewise, if the plasma is very dense, the effects of ion-ion collisions may become important. This can be accounted for by including an extra term in the Lorentz Force Law. In most of the magnetosphere however, the plasma is fully ionized and of low density, and these effects are therefore ignored.

2.3 The Dispersion Relation

From Maxwell's equations and the constitutive relations for the plasma we can derive so called dispersion relations, expressing the relation between the frequency and the wave number of a propagating wave. This relation contains all information about the phase speed of the wave. Let's take a look at the dispersion relation for waves in a warm magnetized plasma:

$$(\frac{\omega}{k})^2 = V_A^2 \cos^2\theta \tag{11}$$

$$(\frac{\omega}{k})^2 = \frac{1}{2}\{V_S^2 + V_A^2 \pm [(V_S^2 + V_A^2)^2 - 4V_S^2 V_A^2 \cos^2\theta]^{\frac{1}{2}}\} \tag{12}$$

where ω is the angular frequency of the wave, $k = 2\pi/\lambda$ is the wave number, θ is the angle between the wave vector and the field magnetizing the plasma in which the wave is propagating, $V_A = |\mathbf{V}_A|$ is the Alfvén speed and V_S the speed of sound in the media. Note that the quotient $\frac{\omega}{k}$ is just the phase speed of the wave.

These relations allows for three different modes of wave propagation. A wave with angular frequency and wave number satisfying relation (11) is a shear Alfvén wave. This wave carries a perturbation magnetic field and a motion of the plasma which is perpendicular to the plane of the wave vector and to the background magnetic field, but does not change the plasma density, plasma pressure or the magnetic pressure. The phase speed of this wave depends on the angle between the wave vector and the background field, as can be seen from equation (11), and all the energy in the wave is carried in a direction parallel to $\mathbf{B}$. If the wave vector is perpendicular to the magnetic field, the phase speed is zero. Thus, this wave cannot propagate perpendicular to $\mathbf{B}$, and will not be of interest.

The other two modes carries changes of plasma density and pressure, and are therefore called compressional waves, and sometimes magnetoacoustic or magnetosonic waves. They may also change the magnetic pressure and the background field magnitude, since the perturbation magnetic field of these waves lie in the plane of $\mathbf{B}$ and $\mathbf{k}$. In contrast to the Alfvén wave, which is a reaction to a disturbance of the magnetic field lines, they act to reduce pressure gradients. We see from equation (12) that if the temperature is zero, so that the speed of sound is zero, we have only one wave propagating with phase speed V_A. If on the other hand B is zero, we have a wave with phase fronts propagating with the speed of sound. Also, if the wave vector

is orthogonal to the magnetic field, so that $\cos\theta = 0$, we have only one wave with phase speed $\sqrt{V_A^2 + V_S^2}$.

A negative sign in (12) gives us the slow mode wave. Slow waves carry energy predominantly along the background field, and so it does not propagate perpendicular to $\mathbf{B}$. Its phase velocity is less than or equal to V_A. Neither this wave will carry any significant amount of energy between the bow shock and the magnetopause.

The positive sign in relation (12) gives the so called fast mode. In this mode the wave energy can propagate in any direction. Its phase speed is higher than or equal to V_A, depending on the direction of propagation relative the background field. This mode is the only one we shall be concerned with hereafter.

These are the simplest kinds of wave propagation in plasma. Other dispersion relations, for other plasma configurations, will allow for different modes of wave propagation. In this work a form of equation (12), proposed by [3], will be used:

$$\omega^{*4} - |\mathbf{k}|^2\{\omega^{*2}(|\mathbf{V}_A|^2 + V_S^2) - (\mathbf{k}\cdot\mathbf{V}_A)^2 V_S\} = 0 \tag{13}$$

where $\omega^* = \omega - \mathbf{k}\cdot\mathbf{V}$ is the angular frequency of the wave seen in the rest frame of Earth, Doppler shifted by the plasma velocity $\mathbf{V}$.

2.4 Modeling of the Background Quantities

There are three main points in the modeling of the background quantities:

- The plasma flow
- The plasma pressure/temperature/density
- The background magnetic field

The plasma flow is considered to be steady and irrotational, i.e.

$$\nabla\cdot\mathbf{v} = 0 \tag{14}$$

$$\nabla\times\mathbf{v} = 0. \tag{15}$$

from the continuity equation. Solving the Laplace equation for a flow around a sphere of radius a, we get the potential function

$$\Psi = -v_0\cos(\theta)(r + \frac{a^3}{2r^2}). \tag{16}$$

This gives the following expressions for the $x-$ and $y-$components of the flow velocity:

$$v_x = -\frac{3v_0a^3}{2}\frac{xy}{(x^2+y^2)^{5/2}} \tag{17}$$

$$v_y = v_0(1 + \frac{a^3}{2}\frac{x^2-2y^2}{(x^2+y^2)^{5/2}}). \tag{18}$$

If we furthermore assume that the flow is inviscid and incompressible, the pressure along a streamline is given by the Bernoulli equation:

$$p + \frac{1}{2}\rho v^2 = const. \tag{19}$$

or

$$p = p_0 + \frac{1}{2}\rho(v_0^2 - v^2). \tag{20}$$

which is the form used in the code. This approximation is realistic near the magnetosheath nose where the flow is subsonic.

Since we are assuming a purely hydrodynamic flow, without considering the electromagnetic properties of the flowing plasma, introducing a magnetic field will inevitably lead to inconsistencies in the model. The best we can do is to investigate the model for a small magnetic field, and try to make a qualitative evaluation of the result.

2.5 General Ray Tracing

I will here give a rudimentary description of the ray tracing methods used in this work. For a complete theory, refer to [10], or, for a more heuristic but thorough treatment, to [11].

For our purposes, we assume that the dispersion relation can be expressed as

$$\omega = \omega(\mathbf{k}, \mathbf{r}),$$

and that the wave can be represented on complex form as (3) where the amplitude Ψ, the phase ϕ and the dispersion relation all vary slowly with the space coordinates $\mathbf{r}$. Furthermore, we assume that the wave is plane, so that the phase function can be written $\phi = \mathbf{k} \cdot \mathbf{r} - \omega t$. The stationary phase condition, (5), then assumes the form

$$\frac{\partial}{\partial \mathbf{k}}[\mathbf{k} \cdot \mathbf{r} - \omega t] = 0, \tag{21}$$

which is equivalent to

$$\mathbf{r} = \frac{\partial \omega}{\partial \mathbf{k}} t, \tag{22}$$

i.e. the wave disturbance, localized to the point $\mathbf{r}$, travels through space with the group velocity $\mathbf{V}_G = \frac{\partial \omega}{\partial \mathbf{k}}$:

$$\frac{d\mathbf{r}}{dt} = \frac{\partial \omega}{\partial \mathbf{k}}. \tag{23}$$

Given the dispersion relations, the equation system (23) thus describes the path of the wave disturbance. The system is not complete, however. To evaluate the right hand side of equation (23) at a point in space, we also need to know the wave vector at that point. We therefore need to find equations for the components of $\mathbf{k}$.

Differentiating the phase function ϕ gives

$$\frac{\partial \phi}{\partial \mathbf{r}} = \mathbf{k} \tag{24}$$

$$\frac{\partial \phi}{\partial t} = -\omega. \tag{25}$$

These equations can then be used to express the dispersion relation as

$$-\frac{\partial \phi}{\partial t} = \omega(\frac{\partial \phi}{\partial \mathbf{r}}, -\mathbf{r}). \tag{26}$$

Differentiation of this with respect to the space variables $\mathbf{r}$, using the chain rule, gives us

$$-\frac{\partial^2 \phi}{\partial \mathbf{r} \partial t} = (\frac{\partial \omega}{\partial \mathbf{k}})^T \cdot \frac{\partial \mathbf{k}}{\partial \mathbf{r}} + \frac{\partial \omega}{\partial \mathbf{r}} \tag{27}$$

Rearranging the terms and using expression (24), we get

$$\frac{\partial \mathbf{k}}{\partial t} + (\frac{\partial \omega}{\partial \mathbf{k}})^T \cdot \frac{\partial \mathbf{k}}{\partial \mathbf{r}^2} = -\frac{\partial \omega}{\partial \mathbf{r}} \tag{28}$$

Since $\mathbf{k}$ is a function of $\mathbf{r}$ and t, the total time derivative of $\mathbf{k}$ can be written, using equations (23) and 28 and transposing the second term

$$\frac{d\mathbf{k}}{dt} = \frac{\partial \mathbf{k}}{\partial t} + (\frac{\partial \mathbf{k}}{\partial \mathbf{r}})^T \cdot \frac{\partial \mathbf{r}}{\partial t} = \frac{\partial \mathbf{k}}{\partial t} + (\frac{\partial \omega}{\partial \mathbf{k}})^T \cdot \frac{\partial \mathbf{k}}{\partial \mathbf{r}} = -\frac{\partial \omega}{\partial \mathbf{r}} \tag{29}$$

This derivative is the rate of change of $\mathbf{k}$ following a point moving with velocity $\mathbf{V}_G = \frac{d\mathbf{r}}{dt}$, which is the point $\mathbf{r}$ in equation (23). Equations (23) and (29) now constitutes a system of coupled ordinary differential equations for the six variables $\mathbf{r}$ and $\mathbf{k}$. They describe the time development of a wave disturbance, traveling along a narrow path as explained above. By differentiating the dispersion relation and solving with respect to $\frac{\partial \omega}{\partial \mathbf{r}}$ and $\frac{\partial \omega}{\partial \mathbf{k}}$, a numerically integrable form of these equations can be obtained, as will be seen in the next section.

2.6 The Ray Tracing Equations

The dispersion relation, introduced in section 2.3, is now used to derive a system of equations for the ray propagation. Differentiation of the dispersion relation (13) with respect to $\mathbf{k}$ gives:

$$\{4\omega^{*3}-2\omega^*|\mathbf{k}|^2(|\mathbf{V}_A|^2+V_S^2)\}\frac{\partial\omega^*}{\partial\mathbf{k}}-2\mathbf{k}\{\omega^{*2}(|\mathbf{V}_A|^2+V_S^2)-(\mathbf{k}\cdot\mathbf{V}_A)V_S^2\} \quad (30)$$

where $\omega^* = \omega - \mathbf{k}\cdot\mathbf{V}$ as before. Solving for $\frac{\partial\omega^*}{\partial\mathbf{k}}$ we obtain

$$\frac{\partial\omega^*}{\partial\mathbf{k}} = \frac{\mathbf{k}\{\omega^{*2}(|\mathbf{V}_A|^2+V_S^2)-(\mathbf{k}\cdot\mathbf{V}_A)^2V_S^2\}-|\mathbf{k}|^2(\mathbf{k}\cdot\mathbf{V}_A)V_S^2\mathbf{V}_A}{\omega^{*2}\{2\omega^*-|\mathbf{k}|^2(|\mathbf{V}_A|^2+V_S^2)\}} \quad (31)$$

Differentiation of the dispersion relation with respect to $\mathbf{r}$ gives

$$\begin{aligned}\{4\omega^{*3}-2\omega^*|\mathbf{k}|^2(|\mathbf{V}_A|^2+V_S^2)\}\frac{\partial\omega^*}{\partial\mathbf{r}}-|\mathbf{k}|^2\{2\omega^{*2}(\mathbf{V}_A\cdot\frac{\partial\mathbf{V}_A}{\partial\mathbf{r}}+V_S\frac{\partial V_S}{\partial\mathbf{r}})-\\ 2(\mathbf{k}\cdot\mathbf{V}_A)^2+V_S\frac{\partial V_S}{\partial\mathbf{r}}-2(\mathbf{k}\cdot\mathbf{V}_A)\mathbf{k}\cdot\frac{\partial\mathbf{V}_A}{\partial\mathbf{r}}V_S^2-2(\mathbf{k}\cdot\mathbf{V}_A)^2V_S\frac{\partial V_S}{\partial\mathbf{r}}\}\end{aligned} \quad (32)$$

which is equivalent to

$$\frac{\partial\omega^*}{\partial\mathbf{r}} = \frac{|\mathbf{k}|^2\{\omega^{*2}(\mathbf{V}_A\cdot\frac{\partial\mathbf{V}_A}{\partial\mathbf{r}}+V_S\frac{\partial V_S}{\partial\mathbf{r}})-(\mathbf{k}\cdot\mathbf{V}_A)V_S^2\mathbf{k}\cdot\frac{\partial\mathbf{V}_A}{\partial\mathbf{r}}-(\mathbf{k}\cdot\mathbf{V}_A)^2V_S\frac{\partial V_S}{\partial\mathbf{r}}}{\omega^{*2}\{2\omega^*-|\mathbf{k}|^2(|\mathbf{V}_A|^2+V_S^2)\}} \quad (33)$$

Using equations (29) and (23) we arrive at

$$\frac{d\mathbf{r}}{dt} = \frac{\mathbf{k}\{\omega^{*2}(|\mathbf{V}_A|^2+V_S^2)-(\mathbf{k}\cdot\mathbf{V}_A)^2V_S^2\}-|\mathbf{k}|^2(\mathbf{k}\cdot\mathbf{V}_A)V_S^2\mathbf{V}_A}{\omega^{*2}\{2\omega^*-|\mathbf{k}|^2(|\mathbf{V}_A|^2+V_S^2)\}}+\mathbf{V}_P \quad (34)$$

$$\begin{aligned}\frac{d\mathbf{k}}{dt} = -\frac{1}{\omega^{*2}\{2\omega^*-|\mathbf{k}|^2(|\mathbf{V}_A|^2+V_S^2)\}}\Big(|\mathbf{k}|^2\{\omega^{*2}(\mathbf{V}_A\cdot\frac{\partial\mathbf{V}_A}{\partial\mathbf{r}}+V_S\frac{\partial V_S}{\partial\mathbf{r}})\\ -(\mathbf{k}\cdot\mathbf{V}_A)V_S^2\mathbf{k}\cdot\frac{\partial\mathbf{V}_A}{\partial\mathbf{r}}-(\mathbf{k}\cdot\mathbf{V}_A)^2V_S\frac{\partial V_S}{\partial\mathbf{r}}\Big)-(\frac{\partial\mathbf{V}_P}{\partial\mathbf{r}})^T\cdot\mathbf{k}\end{aligned} \quad (35)$$

The equations (34) and (35) constitute an explicit system of equations for the ray path, which can be solved by a numerical step-by-step method. In the next chapter we shall see how this can be done.

3 Software Structure and Usage

3.1 Modularization

In building the program, I have tried to modularize it in a way that follows the physical structure of the problem as closely as possibly, both in order to make it intuitive to the user experienced in this field, and to make the various modules easy to replace, should a more advanced model be wished for. The main modules will be separated into different directories, each directory containing various submodules, or files. Each file, in turn, contains the appropriate routines for computing a quantity or performing a task, without getting too dependent on the implementation of the rest of the program.

Firstly, the program is divided into two main parts, which here are called the logic module and the physics module. The logic module contains the routines for creating initial values, the ODE solver algorithm for the ray tracing and its helper functions, and the plotting routines. It also contains the dispersion relation and the expressions for the sound and Alfvén velocities, since these expressions are more or less exact and not likely to be substituted in a future version. If one should wish to do so, these submodules might be moved to the physics module. Furthermore, the logic module contains the boundary models, i.e., the expressions for the coordinates of magnetopause and bow shock. This is more because of convenience than for logical reasons, and one might want to create a separate module out of these, which could be called the geometry module.

The physics module contains functions for computing all the physical quantities involved, given the relevant parameters. These are mass density, mass pressure, magnetic field vector and velocity vector of the plasma flow. The physics module can be replaced without tampering with the logic module. In this work, two physics modules are explored: one with a linear flow, the other with incompressible flow around a sphere.

Each of the two main modules has a separate settings file, where all the actual numerical values controlling the output can be set.

3.2 Geometry and Coordinate Systems

The geometry of the magnetosphere is very dynamic. The barrier that the bow shock presents against the stream of plasma coming from the Sun moves with the changing intensity in the flow, which may alter the distance between the magnetopause and Earth by several Earth radii. This means that there are a number of different geometrical configurations that possibly would be interesting to implement and explore. In this work we are using only one simple model for each of the two boundaries, but the program is implemented in a way to make it easy to change one or both of these.

The bow shock is approximated with a parabola and the magnetopause with a sphere. The distance between Earth and the magnetopause is set to

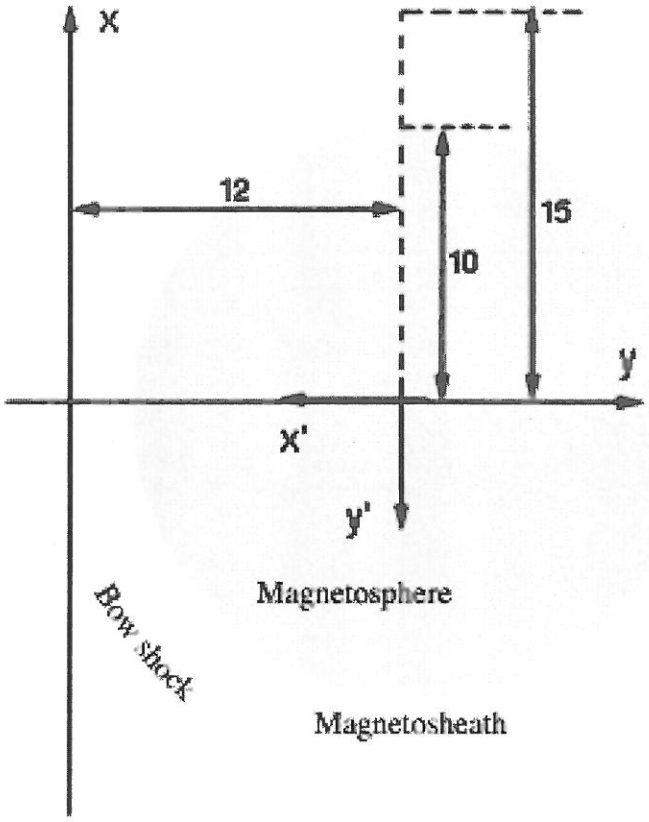

Figure 2: Ray tracing coordinate systems

10 Earth radii along the Sun-Earth line, and 15 Earth radii in the direction perpendicular to this line. We assume that the solar wind is parallel to the Sun-Earth axis. We are looking at the equatorial plane, and assume that the magnetic field is everywhere perpendicular to this plane.

For the ray tracing algorithms we are using a coordinate system with the origin fixed at the subsolar point on the bow shock, the x-axis pointing in the direction of Earth's motion around the Sun, the y-axis pointing towards Earth, and the z-axis completing a right-handed system. The flow model is for simplicity of the equations using a different coordinate system: origin fixed at the center of Earth, y-axis pointing towards the Sun, and the x-axis in the counter-direction to Earth's motion around the Sun. The transformation from the flow coordinates to the ray tracing coordinates is thus a displacement by 10 Earth radii along the y-axis of the first of these systems.

For clarity, the paths of the incident rays are plotted a short distance before they hit the bow shock. This is done with no intention of actually simulating the ray propagation outside the bow shock, but merely to make the angle of incidence and the forms of the incident wave fronts clear in the

plots. To initiate the incident rays, we use yet another coordinate system: origin fixed on a point on the Earth-Sun axis between the Sun and the bow shock, with the axes turned an angle θ, the angle at which the wave hits the bow shock, in relation to the coordinate axes of the ray tracing system described above. The transformation from the coordinates of the initial rays to the ray tracing coordinates is thus a displacement along the negative y-axis of the ray tracing system, and a rotation with an angle θ.

In the program code, these transformations are executed inside the modules for computing the flow vector and the incident ray, respectively. In the main routines, we always assume the ray tracing coordinate system, hereafter called the main coordinate system.

3.3 Initializing the Ray

In the settings file of the logic module, a number of parameters for configuring an initial set of rays are available. The rays are initialized at the bow shock, and traced from there until they hit the magnetopause. To compute the phase of a ray at the point where it hits the bow shock, a straight path AB is tracked backwards from the bow shock to the line AC making an angle θ with the Sun-Earth line, see figure 2. We assume that a plane phase front hits the line AC at time $t = 0$. Elementary vector algebra gives the length of the distance AB, which is the distance the phase front has traveled since $t = 0$ until it hits the bow shock:

$$\overrightarrow{CB} = \overrightarrow{OB} - \overrightarrow{OC} \tag{36}$$

$$\overrightarrow{CA} = (\overrightarrow{CB} \cdot \mathbf{e}_{x'})\mathbf{e}_{x'} \tag{37}$$

$$\overrightarrow{AB} = \overrightarrow{CB} - \overrightarrow{CA}, \tag{38}$$

where $\mathbf{e}_{x'}$ is the unit vector in the coordinate system of the incident wave, see the section about geometry and coordinate systems. The time it takes for the phase front to get from A to B is computed by using the phase speed

$$V_P = \frac{\omega}{k} \tag{39}$$

where k is the wave number and ω the angular frequency of the incident wave.

The initial values are returned as an $n \times 7$-matrix, where each row represents one initial ray vector. The first entry in each row is the time when that ray hits the bow shock, the three following entries are the coordinates of the crossing point and the last three entries are the wave vector at the bow shock. By taking one of these rows at a time as initial vector and solving the equations step by step until the halting condition is met, the ray paths are computed.

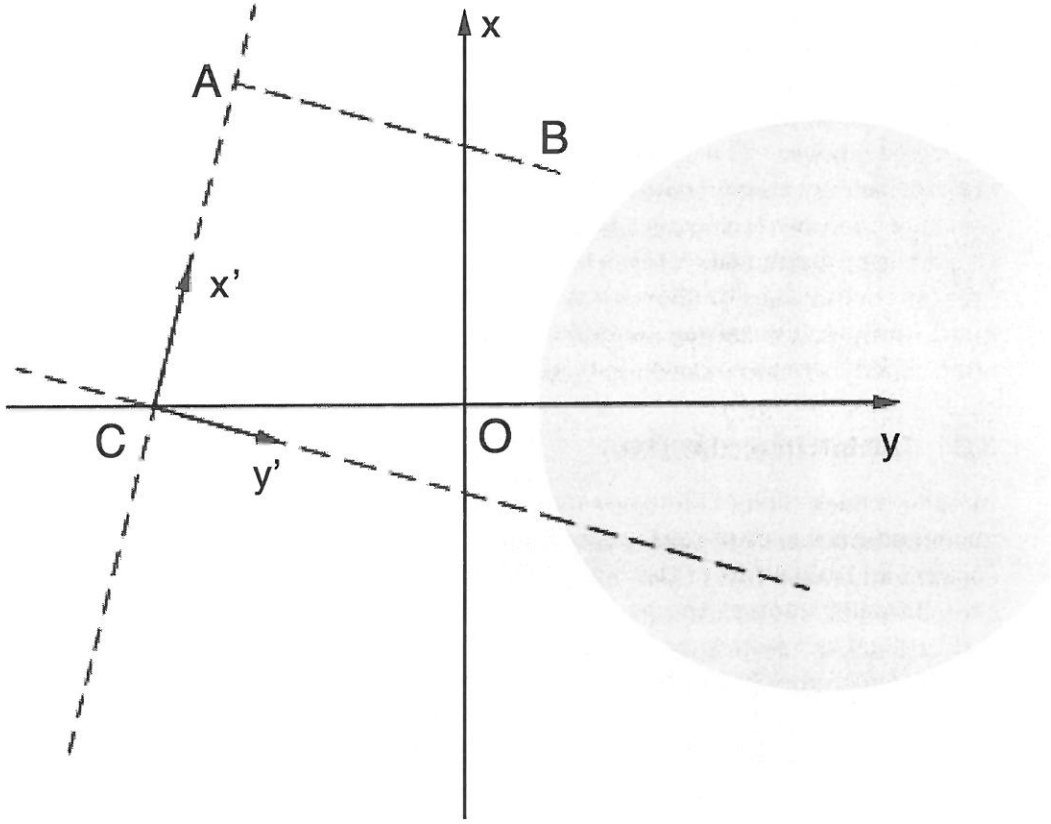

Figure 3: Ray tracing coordinate systems.

3.4 The Ray Tracing Algorithm

The ray tracing is, in short, performed by solving the system of ordinary differential equations (34) and (35), using the IDL implementation of the Runge-Kutta fourth order method and a step halving algorithm for error control. The routines for this task are located in the file `ode_solver.pro`. They are not specifically adopted to the immediate problem, and it should be quite possible to use them to solve other systems of ODE's.

To run the program, values for the time step size and the local error tolerance are chosen in the settings file `raytrsettings.pro`. Conditions for halting the program execution are chosen by giving the name of a boolean function that will be evaluated after each time step, with the current solution as argument. In this way, we can choose to halt execution after a specified number of time steps, when the ray hits the magnetopause, when a quantity blows up numerically, or when some other condition of our choice is fulfilled. The program is compiled by running the file `raytr.compile`, and executed with the file `raytr.run`. Every execution of the program results in a plot of

the paths of a set of rays through the equatorial plane of the magnetosheath.

The error control method is is a simple Richardson extrapolation. If $S, S_{\Delta t}$, and $S_{\Delta t/2}$ indicate the exact solution, the numerical solution with a time step size Δt, and the solution with a time step size $\frac{\Delta t}{2}$ respectively, the error $E_{\Delta t}$ can be estimated by the following computation, since the method used is fourth order:

$$S = S_{\Delta t} + E_{\Delta t} = S_{\Delta t/2} + \frac{1}{16} E_{\Delta t} \Rightarrow \tag{40}$$

$$|E_{\Delta t}| = \frac{16}{15} |S_{\Delta t} - S_{\Delta t/2}| \tag{41}$$

Another way of controlling the error is to check how well the solution satisfies the local dispersion relation. If the expression 13 is not close enough to zero, the solution is recalculated, using a smaller time step. This method has the advantage of being considerably faster, since the step halving doesn't have to be performed in each time step. Figure 10 gives some hint on the connection between the errors in $\mathbf{r}$, $\mathbf{k}$ and the dispersion relation.

To correct the error, the program utilizes an adaptive step size method. This method is controlled by five parameters in the `raytrsettings.pro` file: `red_fact`, the factor with which the step size is reduced if the error is larger than acceptable; `exp_thr`, the minimal error beneath which the step size will be expanded; `exp_fact`, the factor with which the step size is expanded if the error is less than `exp_thr`; `min_dt`, `max_dt` and `initial_dt`, the minimal, maximal and initial time steps respectively.

Though a lot of simplifications could have been performed due to the assumptions about the direction of the background magnetic field already made, the actual equations are implemented in a general fashion, following exactly the formulas (34) and (35). Apart from facilitating further development, it turned out to be more time effective, since the computations could be executed using vector algebra.

3.5 What Happens at the Bow Shock

A wave incident on the bow shock will be transmitted and reflected, fulfilling certain laws and boundary conditions, which affect the direction, the amplitude and the polarization of the wave. In this work we are only considering refraction by Snell's law, expressed as $\mathbf{e}_n \cdot \mathbf{k}_i = \mathbf{e}_n \cdot \mathbf{k}_t$, where $\mathbf{e}_n$ is the unit vector normal to the bow shock, $\mathbf{k}_i$ is the wave vector of the incident wave and $\mathbf{k}_t$ the wave vector of the transmitted wave. This tells us that the tangential component of the wave vector is constant across the boundary. The other component of the transmitted wave vector is chosen to satisfy the dispersion relation inside the bow shock. For a more detailed treatment of reflection and transmission at the bow shock, refer to [3]

The incident wave vector is assumed to be constant along the bow shock. Its frequency ranges from 0.001 Hz (Pc-5) to 0.1 Hz (Pc-3). Outside the bow

shock, the flow velocity of the plasma is typically higher than the sound and Alfvén speeds (see figure 11 for some typical values). The wave fronts are therefore mainly convected towards the bow shock with the speed V of the plasma flow, and the wave number k and frequency f of the incident wave satisfies the simple dispersion relation $kV = 2\pi f$. The phase speed (and wavenumber) of the transmitted wave, on the other hand, is dependent on the values we choose for the background quantities inside the bow shock. Since the flow speed of the plasma is considerably lower at the nose region, the sound and Alfvén speeds becomes significant.

3.6 Plotting the Result

The solution, the time development of a single initial vector $(t_0, \mathbf{r}_0, \mathbf{k}_0)$, is returned as an $m \times 7$-matrix, where each row $(t_i, \mathbf{r}_i^T, \mathbf{k}_i^T)$ represents one time step, from the bow shock until it either hits the magnetopause or the plasma flow speed becomes supersonic, where the incompressible flow assumption breaks down. This process is repeated for a set of rays, and each ray path is plotted. By indicating lines of constant phase, the wave fronts are visualized as they propagate through the magnetosheath. At the same time, one can see the direction of energy propagation, since the energy flux is along the ray paths. Where the paths diverge, the energy density decreases, and vice versa.

To visualize the wave fronts incident on the bow shock, the ray paths are extrapolated backwards from the bow shock to the starting point at $t = 0$, assuming constant values everywhere. As earlier mentioned, this is not to study the propagation outside the bow shock, but merely to clarify the picture.

4 Results and Discussion

4.1 Relevance and Consistency of Program Output

The picture of the magnetosheath here presented is extremely simplified, and so it is difficult to draw any conclusions about the actual behaviour of the propagating wave fronts from the program output. We can, however, try to assert that the model is to some degree self-consistent and well behaved. This can then be used as a starting point for further investigations.

The plane wave fronts hit the bow shock, are refracted and propagate deformed through the magnetosheath until they hit the magnetopause or the sonic line, where the simulation is interrupted. In the Earth frame of reference, the wave fronts are moved closer to each other as they cross the bow shock, since the plasma flow speed decreases and the density increases. Figures 4 to 6 show the results for a configuration of typical values, taken from [6], for different angles of incidence. The background values are plotted

in figure 11 across the bow shock and some distance into the magnetosheath. The solid lines in the plots show the ray paths, and the marks on the lines indicate values of constant phase.

In figures 5 and 7, the same configuration of background values has been used, except that the mass density is slightly higher in figure 7. With a higher density, the wave fronts move more slowly through the plasma, as the Alfvén speed is decreased according to 1, which can be seen in the figure. We can also see that the ray paths are more deflected at the bow shock, since the density step is higher. In figure 9, the background magnetic field is increased, which slightly increases the Alfvén speed.

Values of the sound speed, the plasma flow speed and the group speed of the propagating waves are all plotted along two different ray paths in fig 13. In the lower panel a ray path starting close to the bow shock nose is followed, while the upper panel shows values along a path starting further out along the flank. The sound speed is rising in the upper panel and dropping in the lower. This is reasonable since the pressure should be rising across the magnetosheath nose and dropping along the flanks, and the density is constant.

The flow speed follows the opposite pattern, gaining speed along the flanks, as is expected of a gas flow around a circular object.

The group speed along the path starting at the bow shock front rises steadily from around 300 to 400 km/s across the magnetosheath.

To test the ODE-solver and to achieve visual indications on the correctness of the background flow, the program has been used to track the flow lines of the plasma itself, resulting in figure 12.

4.2 Suggestions for Further Work

There are a few obvious improvements to the program that could be easily carried out.

1. The density is here taken as linear in y and independent of all other coordinates. To retain consistency throughout the region, we have to assume constant density. A better model would be to use the fact that the normal component of the flow velocity times the density is constant across the bow shock. This would give a density curve along the bow shock, which then is carried with the flow, so that the density is constant along a flow line. Temperature curves can then be plotted and compared to the results of [7].

2. In this work, the bow shock is approximated as a parabola and the magnetopause as a sphere. The geometry of the magnetosheath could be more accurately modeled by implementing other models for the bow shock and magnetopause positions. For the bow shock, one could

utilize the expression used by [6]

$$\frac{23.3}{R} = 1 + 1.16\cos(\theta). \tag{42}$$

The numerical values in this formula represents the mean position. R is measured in Earth radii from a point three Earth radii towards the Sun. The magnetopause can be more accurately modeled using the equation

$$\frac{dr}{d\phi} = r\Big(\frac{r^6 \sin\phi\cos\phi + r_S^3\sqrt{r^6 - r_S^6}}{r^6\cos^2\phi - r_S^6}\Big) \qquad \frac{\pi}{2} < \phi < \frac{3\pi}{2} \tag{43}$$

also used by [6]. This equation is based on pressure balance considerations and contains the distance r_S between Earth and the magnetopause along the Sun-Earth axis. All routines for the geometry models ae located in the modules `bowshock.pro` and `magnetopause.pro`. It should be possible to substitute these modules separately, without interfering with the rest of the program.

3. Since the ODE solving algorithm, with the error control and adaptive step size method, was written by the author of this report, in a rather short time, it is not very effective, compared to the advanced methods available. If for example the numerical computing language Matlab had been used instead of IDL, the whole `ode_solver.pro` module would have been unnecessary, and the program would have been considerably more time effective. If one wishes to develop the program further, introducing more advanced, and time consuming, models for the background quantities, it would be a good idea to port the whole program to Matlab for this reason.

4. A stability and consistency analysis of the method has to be performed, to make sure that the method converges. Refer to [12] for a thorough treatment of this procedure.

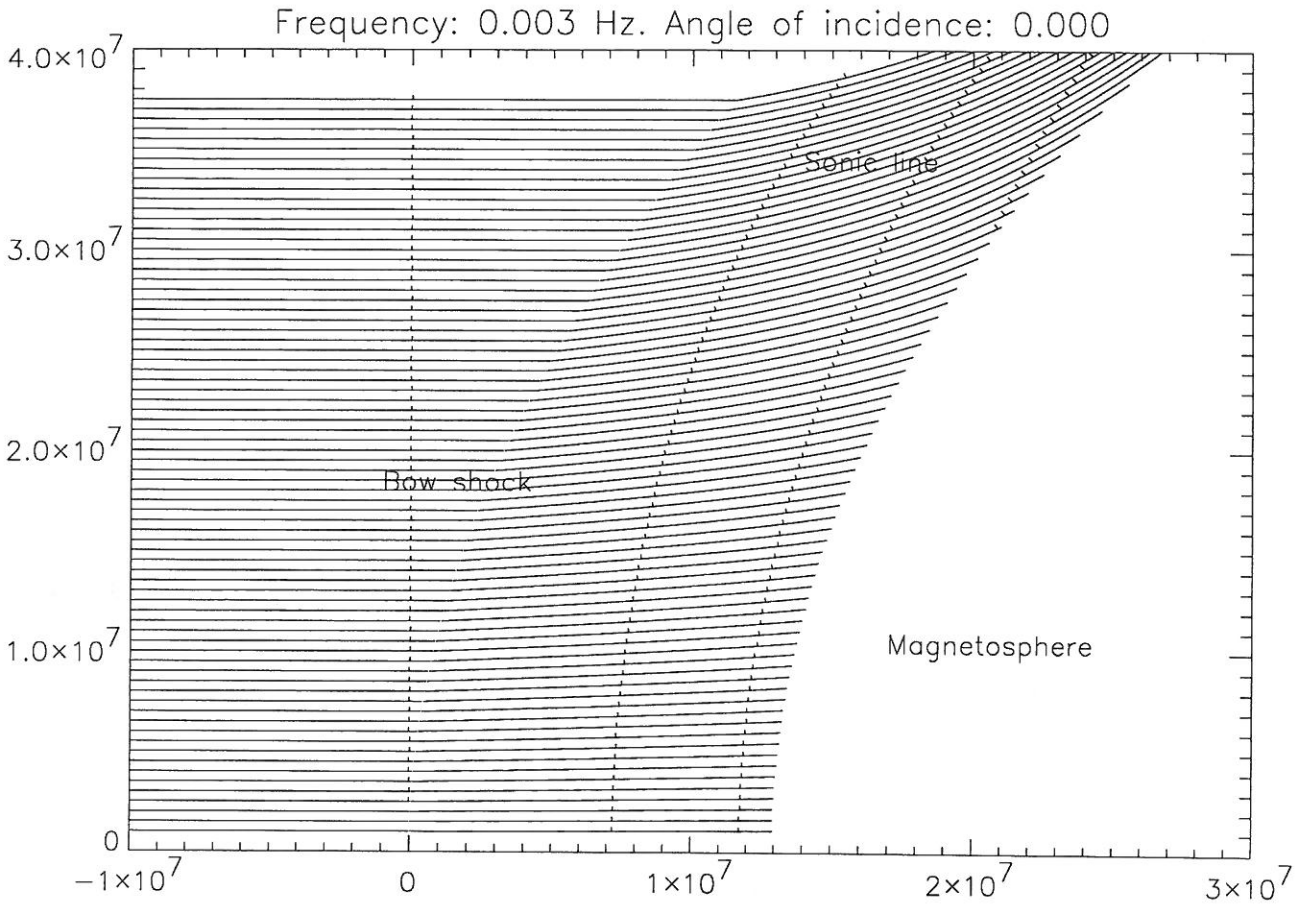

Figure 4: $B = 0$, $\rho = 6.4 \cdot 10^{-21}$

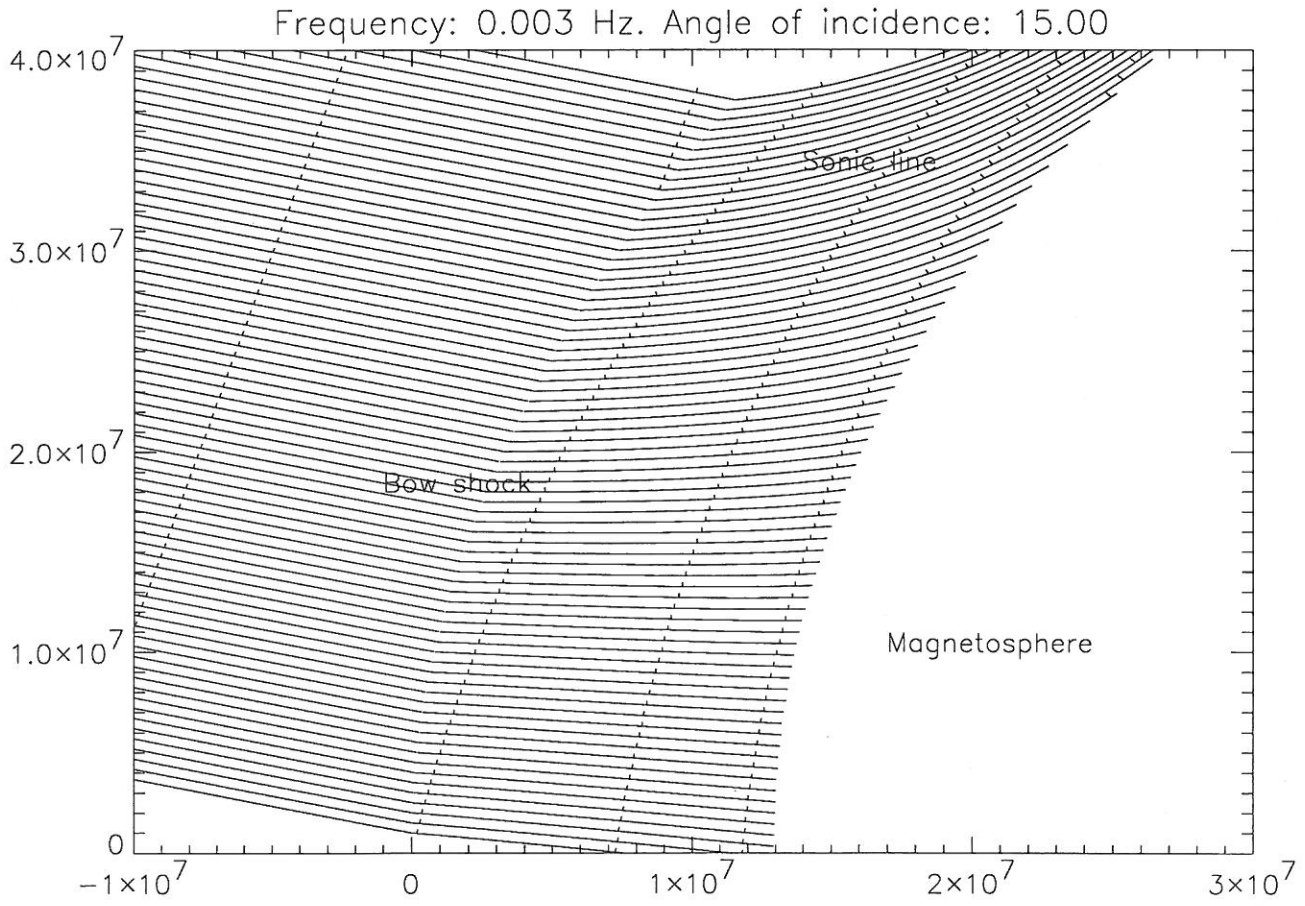

Figure 5: $B = 0$, $\rho = 6.4 \cdot 10^{-21}$

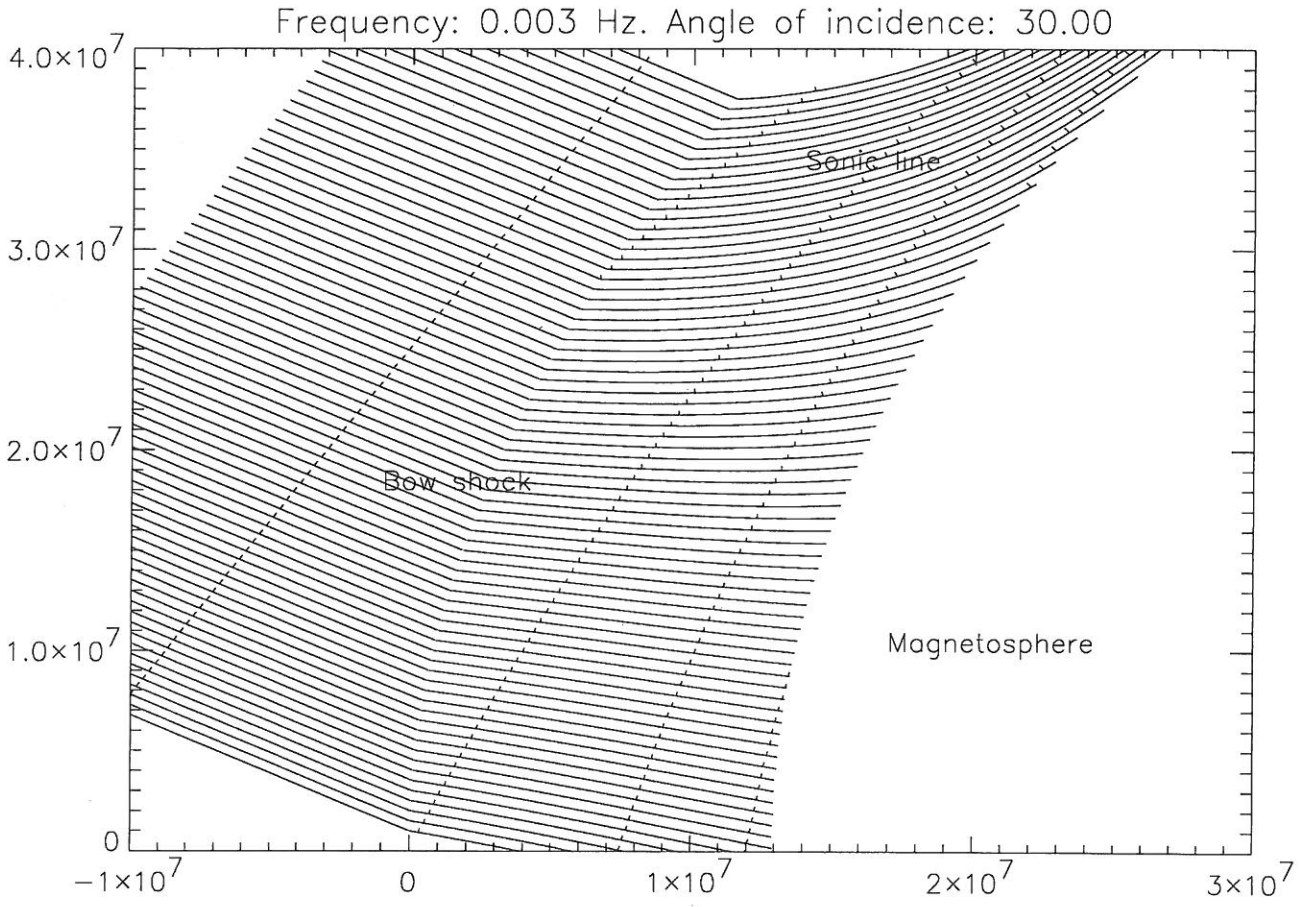

Figure 6: $B = 0$, $\rho = 6.4 \cdot 10^{-21}$

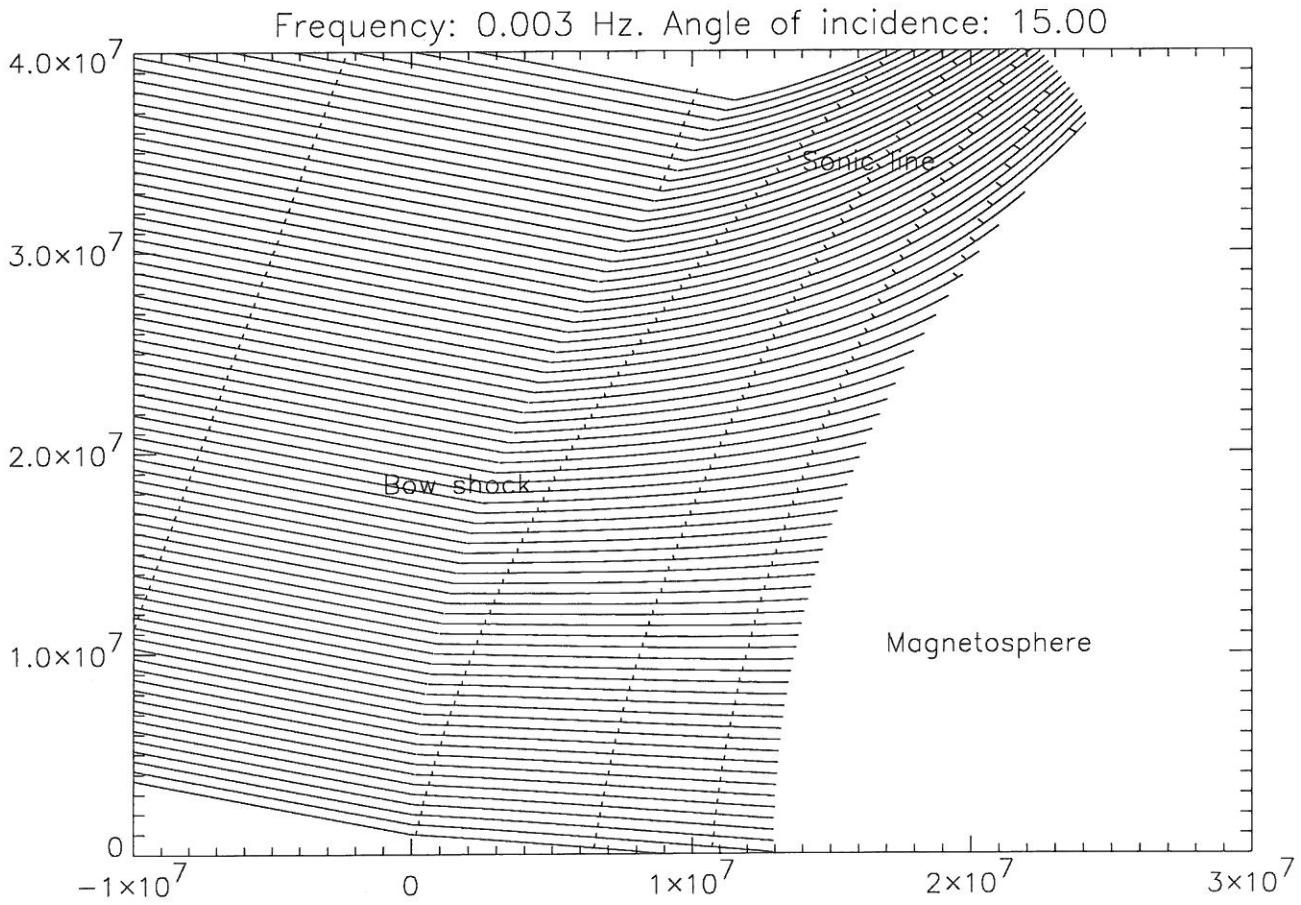

Figure 7: $B = 0$, $\rho = 10^{-20}$

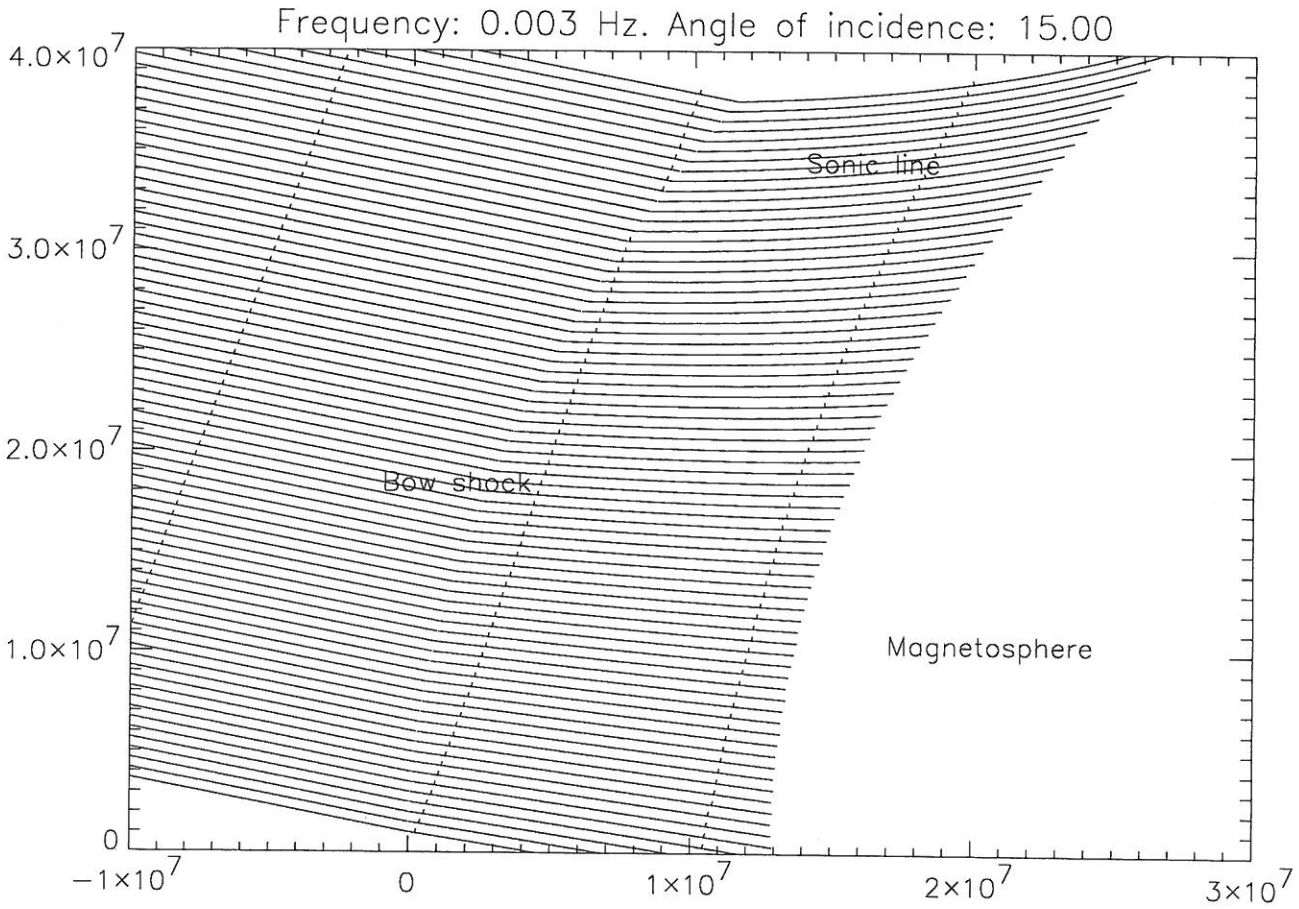

Figure 8: $B = 0$, $\rho = 2.0 \cdot 10^{-21}$

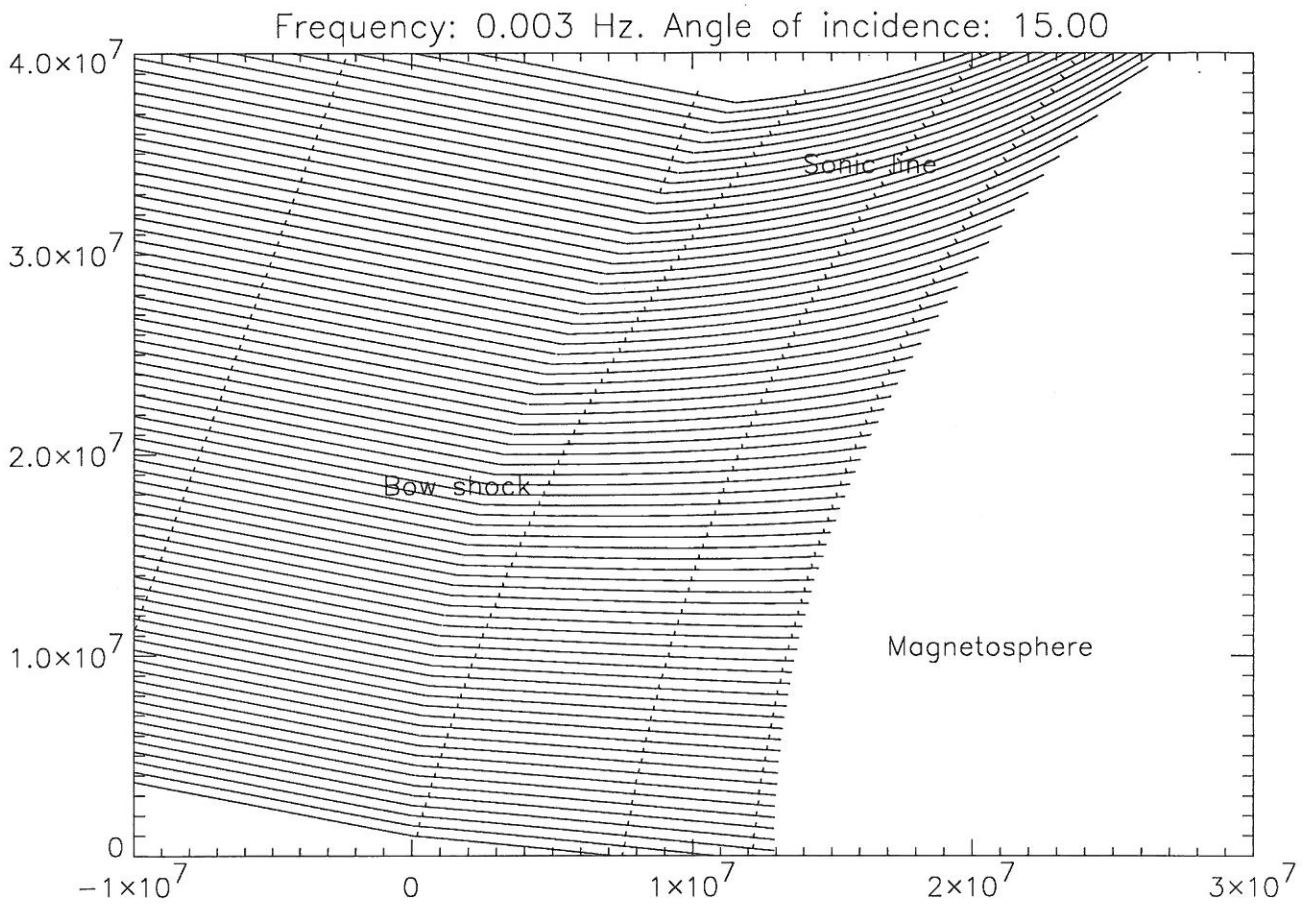

Figure 9: $B = 20$, $\rho = 6.4 \cdot 10^{-21}$

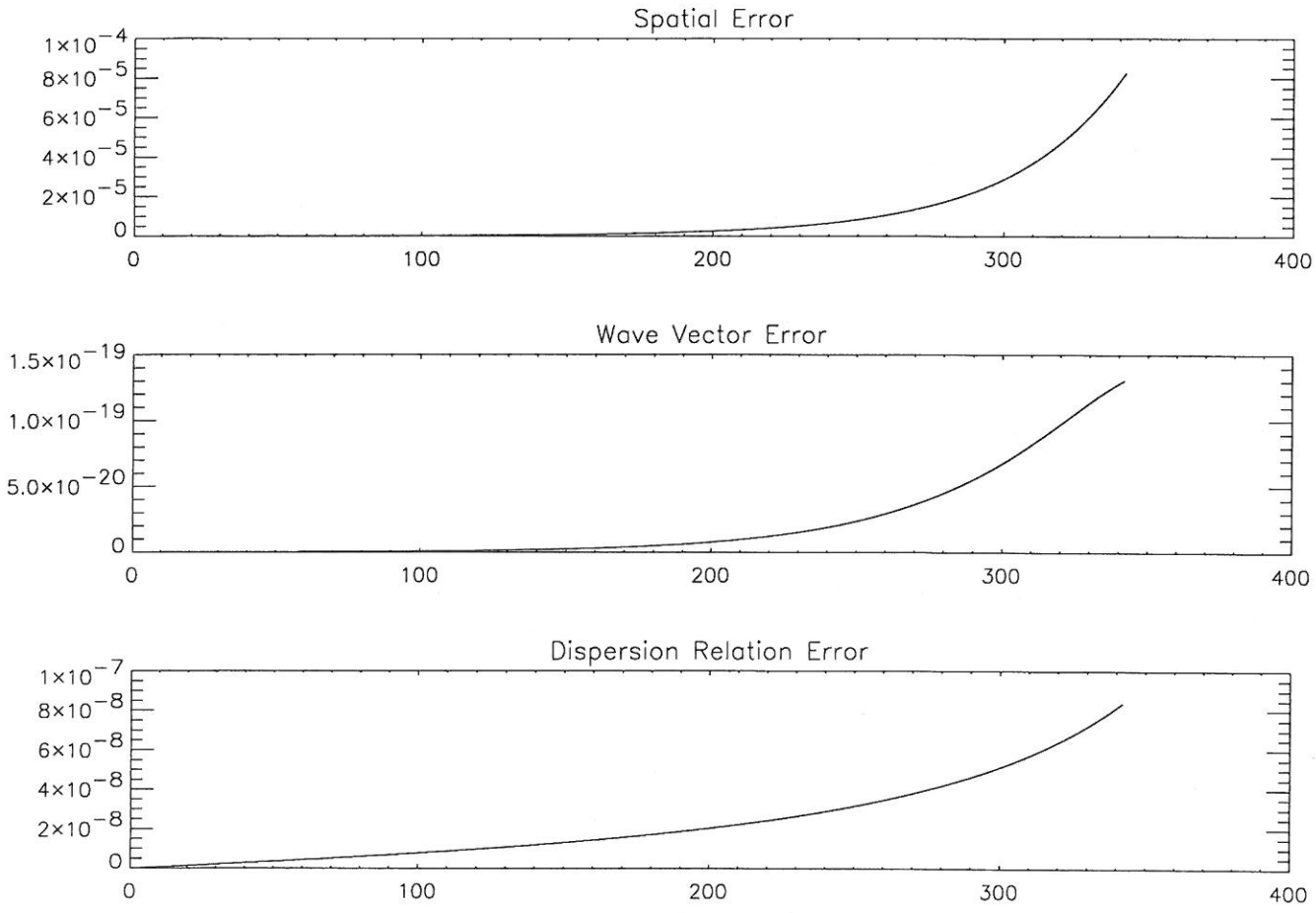

Figure 10: Local error estimation along one ray path

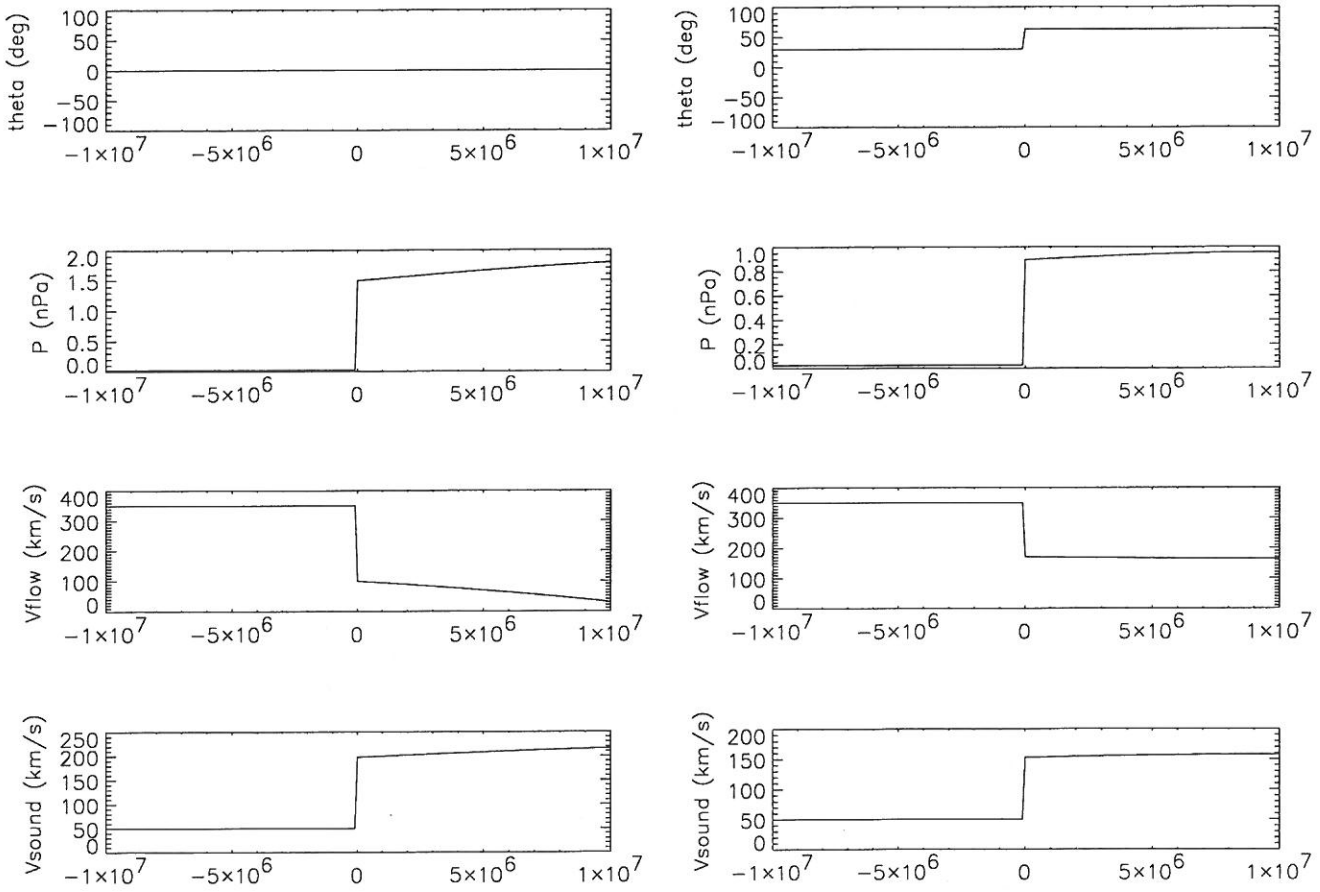

Figure 11: Bow shock values. Left: angle of incidence 0°, right: angle of incidence 30°

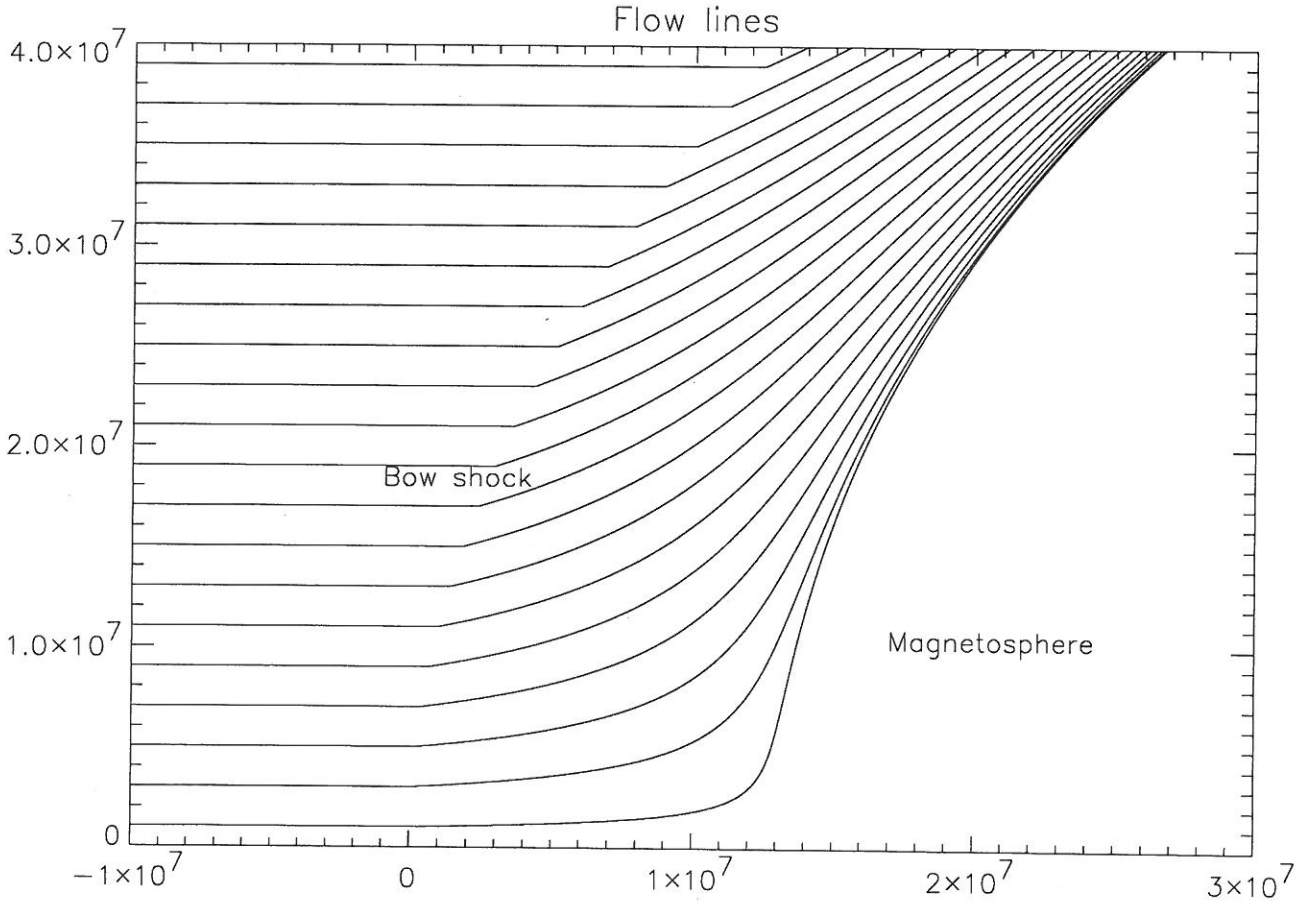

Figure 12: Stream lines for plasma flow

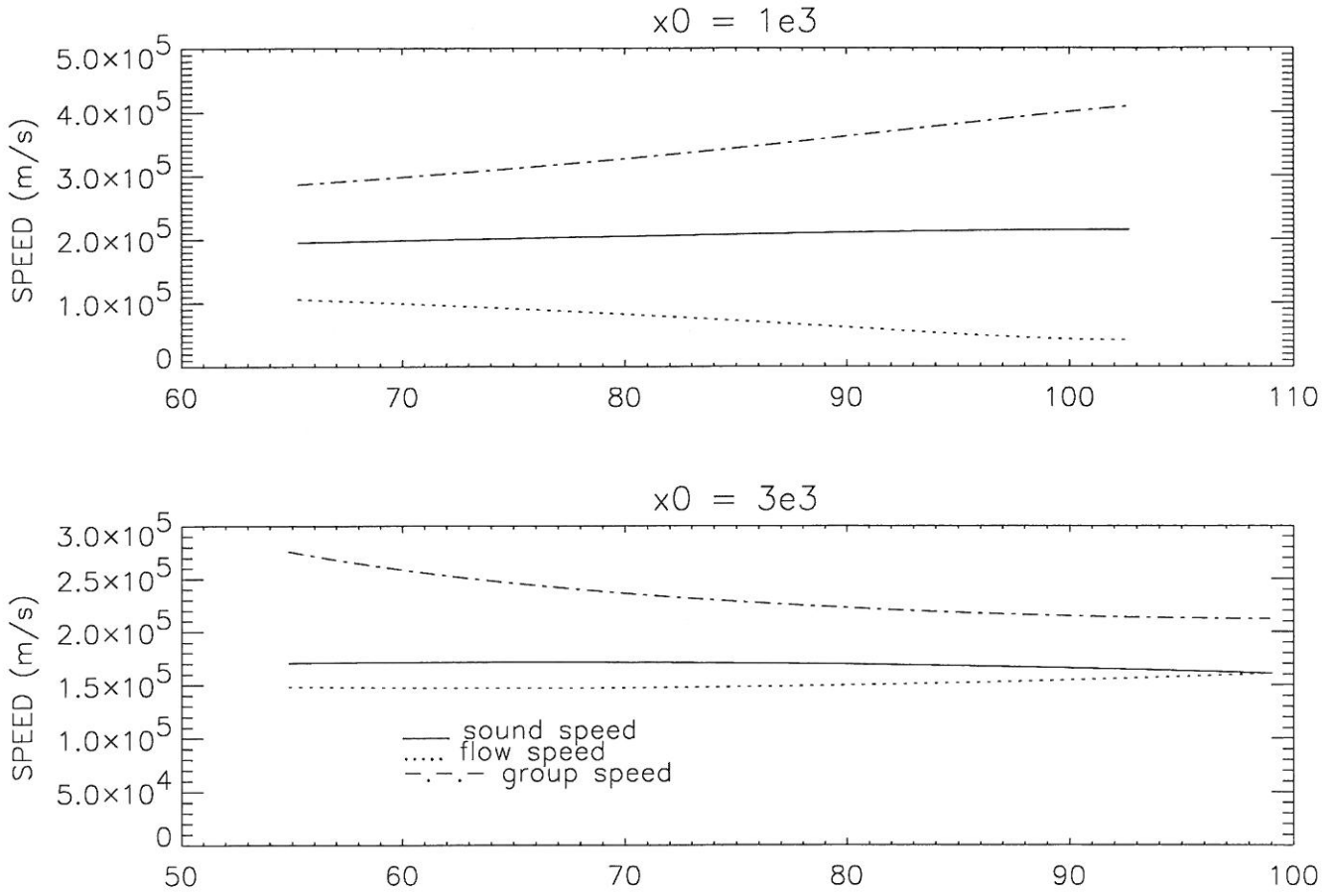

Figure 13: Values along ray path

References

[1] Walker. Excitation of magnetohydrodynamic cavities in the magnetosphere. Journal of Atmospheric and Solar-Terrestrial Physics 60 1998.

[2] Walker. Coupling between waveguide modes and field line resonances. Journal of Atmospheric and Solar-Terrestrial Physics 62 2000.

[3] Walker. Reflection and transmission at the boundary between two counterstreaming plasmas; active boundaries or negative energy waves? Journal of Plasma Physics 63. 1998.

[4] Walker. Wave energy propagation in drifting plasmas. International Journal of Geomagnetism and Aeronomy 2 2000.

[5] Stephenson and Walker. HF radar observations of Pc5 ULF pulsations driven by the solar wind. Geophysical Research Letter 10 2002.

[6] Walker. Excitation of field line resonances by MHD waves originating in the Solar Wind. Journal of Geophysical Research 107 2002.

[7] Spreiter et. al. External Aerodynamics of the Magnetosphere. Space Sciences Division, Ames Research Center, NASA, Moffett Field, Calif., U.S.A.

[8] Potemra and Blomberg. A survey of Pc5 pulsations in the dayside high-latitude regions observed by Viking. Journal of Geophysical Research 101 1996.

[9] Lighthill, J. Waves in Fluids. Cambridge University Press 1978.

[10] Budden, K.G. The propagation of radio waves. Cambridge University Press 1985.

[11] Walker. Plasma waves in the Magnetosphere. Springer Verlag 1993.

[12] Hirsch, C. Numerical Computation of internal and external flows. John Wiley & Sons 1998.

[13] Samson, J. C. Geomagnetic Pulsations and Plasma Waves in the Earth's Magnetosphere. Academic Press Limited 1991.

[14] Stahara, S. Adventures in the magnetosheath: two decades of modeling and planetary applications of the Spreiter magnetosheath model. Planetary and Space Science 50.